Progressive Characterization of Visual Phenotype in Bardet-Biedl Syndrome Mutant Mice

Viola Kretschmer,[1] Sarita Rani Patnaik,[1] Friedrich Kretschmer,[2] Mira Manilal Chawda,[3] Victor Hernandez-Hernandez,[3,4] and Helen Louise May-Simera[1]

[1]Cilia Cell Biology, Institute of Molecular Physiology, Johannes Gutenberg University, Mainz, Germany
[2]Scientific Computing Facility, Max Planck Institute for Brain Research, Frankfurt, Germany
[3]Genetics and Genomic Medicine Programme, Great Ormond Street Institute of Child Health, University College London, London, United Kingdom
[4]Department of Life Sciences, College of Health and Life Sciences, Brunel University London, London, United Kingdom

Correspondence: Helen Louise May-Simera, Institute of Molecular Physiology, Johannes Gutenberg University, Johann-Joachim-Becher-Weg 13-15, Raum 1-521, Mainz 55128, Germany;
hmaysime@uni-mainz.de.

Submitted: July 6, 2018
Accepted: February 17, 2019

Citation: Kretschmer V, Patnaik SR, Kretschmer F, Chawda MM, Hernandez-Hernandez V, May-Simera HL. Progressive characterization of visual phenotype in Bardet-Biedl Syndrome mutant mice. *Invest Ophthalmol Vis Sci*. 2019;60:1132–1143. https://doi.org/10.1167/iovs.18-25210

Purpose. Bardet-Biedl syndrome (BBS) is an archetypical ciliopathy caused by defective ciliary trafficking and consequent function. Insights gained from BBS mouse models are applicable to other syndromic and nonsyndromic retinal diseases. This progressive characterization of the visual phenotype in three BBS mouse models sets a baseline for testing therapeutic interventions.

Methods. Longitudinal acquisition of electroretinograms, optical coherence tomography scans, and visual acuity using the optomotor reflex in *Bbs6/Mkks*, *Bbs8/Ttc8*, and *Bbs5* knockout mice. Gene and protein expression analysis in vivo and in vitro.

Results. Complete loss of BBS5, BBS6, or BBS8 leads to different rates of retinal degeneration and visual function over time. BBS8-deficient mice showed the fastest rate of degeneration, and BBS8 seems to be required for cone photoreceptors to reach functional maturity. In contrast, the loss of BBS5 (a further BBSome component) showed very little degeneration. Loss of BBS8 versus BBS5 resulted in different physiologic responses both in vivo and in vitro. BBS6-deficient mice show a slower rate of degeneration with both rod and cone function reducing at a similar rate.

Conclusions. The mouse models analyzed show distinct and diverging courses of degeneration upon loss of BBS5, BBS6, or BBS8, which can be used as a benchmark to test therapeutic interventions. Close consideration of the different phenotypes reveal subtle but important differences relating to their function. Because we also see differences in terms of phenotype depending on the type of visual assessment used, our data highlight the importance of using a combinatorial approach for assessment of visual function.

Keywords: Bardet-Biedl syndrome, BBSome, primary cilia, retinal disease, mouse mutants

The Bardet-Biedl Syndrome (BBS) belongs to a group of genetic disorders collectively termed ciliopathies. Symptoms include obesity, polydactyly, cognitive disabilities, renal cysts, and most commonly retinal degeneration.[1,2] BBS is caused by mutations in at least one of 21 identified genes, which code for proteins associated with the structure and function of the primary cilium.[1] The primary cilium is a microtubule-based protrusion of the cell membrane, which is known to influence several intracellular signaling pathways as well as transduction of different forms of sensory information from the extracellular environment. Because there is no protein translation machinery inside the cilium, all proteins need to be transported from the cytoplasm. This ciliary trafficking is mediated by a complex of eight BBS proteins (BBS1, BBS2, BBS4, BBS5, BBS7, BBS8/TTC8, BBS9, and BBS18) termed the BBSome.[3–7] The assembly of this complex is facilitated by the BBS chaperonin complex composed of three BBS proteins (BBS6/MKKS, BBS10, and BBS12).[8–10]

Similar to other symptoms, the rate of retinal degeneration varies among ciliopathy patients, without a distinguishable genotype to phenotype correlation. In humans, deleterious variants in the genes coding for the BBS chaperonin complex proteins lead to more severe phenotypes.[11] Some mutations in BBS6/MKKS result in BBS with retinal degeneration, whereas others result in McKusick-Kaufman syndrome which is a disorder with primarily genitourinary malfunctions rather than retinal degeneration.[8,12]

The mammalian photoreceptor is highly sensitive to defects in ciliary trafficking because the entire outer segment (OS) and connecting cilium (CC) is composed of a highly specialized primary cilium.[13,14] All proteins necessary for phototransduction must be trafficked through the CC to reach the OS. Therefore, any defect or disruption in ciliary trafficking has huge consequences for photoreceptor homeostasis leading to cell death and, subsequently, retinal degeneration.[14]

The vertebrate eye has many other ciliated cell types.[14] An additional cell type particularly important for function and maintenance of photoreceptor health is the retinal pigment epithelium (RPE). Long microvilli extend from the apical surface of the RPE and wrap around the photoreceptor OSs and ensure transport of nutrients, visual pigment regeneration, and phagocytosis of shed OSs.[15] It has recently been shown

that the primary cilium is important for maturation of the RPE via regulating signaling pathways during its development.[16] Therefore, it is feasible that BBS patients experience an amplifying effect of diminished support from the RPE in combination with the defective trafficking across the photoreceptor CC, resulting in severe retinal degeneration.

Various therapeutic approaches for the treatment of retinal degeneration in ciliopathies are currently being developed and commonly include gene therapy and pharmacologic advances.[17,18] Because BBS mouse models nicely recapitulate the human disease phenotype, they are increasingly used to develop treatment strategies. Therefore, there is a critical need to better understand the progression of visual dysfunction in these disease models. This knowledge will shed light on the disease mechanisms and help to optimize treatment strategies.

The objective of this study was to progressively characterize the retinal phenotype among three different BBS mouse models over a timespan of 10 months in an effort to gain insight into different molecular functions and effects of ciliopathy-causing genes and to determine a baseline on which therapeutic interventions can be tested.

We focused on the *Bbs8* knockout mouse because patients and mouse models with *BBS8* mutations exhibit a more pronounced phenotype.[19] We also chose to characterize the *Bbs5* knockout mouse because BBS5 has been shown to be involved in translocation of arrestin1 (Arr1) during phototransduction.[20] Finally, the *Mkks/Bbs6* knockout mouse was also chosen to study differences in effect of the loss of BBSome proteins versus chaperonin proteins.

Materials and Methods

Animals

Bbs5 knockout mice were developed by the International Mouse Phenotyping Consortium.[21] *Bbs6* and *Bbs8* knockout mice have been previously described.[22,23] All animals were housed in a 12 hour/12 hour light/dark cycle with food and water available ad libitum. Animal handling and manipulation were performed in accordance with institutional guidelines for animal welfare, German animal protection law, and the ARVO Statement for the Use of Animals in Ophthalmic and Vision Research. Mice were examined every 30 days starting at postnatal day 25 (P25) until a maximum of 12 months. Homozygous $Bbs5^{-/-}$, $Bbs6^{-/-}$, $Bbs8^{-/-}$ and $Bbs5^{+/+}$, $Bbs6^{+/+}$, $Bbs8^{+/+}$ littermate mice were selected by genotyping from heterozygous crosses. Genotyping was performed as previously described. Genotyping primers were used as follows:

- *Bbs6* forward: TACAGAGGCACCTGGCTACC,
- *Bbs6* reverse: TCCTGTGGCATTATGGGTCT,
- *Bbs6* trapping cassette: AAATGGCGTTACTTAAGC TAGCTTGC,
- *Bbs8* wildtype (WT) forward (F): CCGGCAGAACAAACTG TATTGGT,
- *Bbs8* WT reverse (R): TGCTGGCATTTAATGAGGAAGCGTC,
- *Bbs8* knockout F: CCTGGCGGAGGGAATAAAAAG,
- *Bbs8* knockout R: CGTCCTTGAAGAAGATGGTGCG,
- *Bbs5* F: GGTGTCACACATGTCTGACAGTATC,
- *Bbs5* R: AAAAGGTAGTATTGGCCTCGAATTTAC.

Electroretinograms (ERGs)

Mice were dark adapted for 12 hours and anesthetized under red light conditions via intraperitoneal injection of ketamin (87.5 mg/kg) and xylazine (12.5 mg/kg). Eye drops containing 1% tropicamide and 2.5% phenylephrine were applied to ensure pupil dilation. Full-field ERGs were recorded using an Espion V6 Diagnosys system (Diagnosys LLC, Lowell, MA, USA). Gold electrodes (Diagnosys) were placed on the corneal surface of both eyes and referenced to needle electrodes (Diagnosys) between the ears and in the tail as ground. To ensure electrical contact and corneal integrity a drop of 2% methylcellulose was applied to the eye. Mice were placed on a heating pad (37°C) under the ColorDome (Diagnosys) and subjected to light stimulation.

The a- and b-waves were recorded using a dark-adapted protocol of six escalating light flashes (0.0001, 0.001, 0.01, 0.1, 1, and 10 cd s/m^2). For the light-adapted protocol, flashes of 0.3, 1, 3, 10, 30, and 100 cd s/m^2 were used as stimulation, followed by a 10-Hz flicker stimulus of 100 cd s/m^2. The a-wave was determined by measuring the peak of the first negative wave. The b-wave was calculated from the trough of the a-wave to the peak of the first positive wave or from baseline if no a-wave was present.

Data were analyzed and displayed using Matlab (The MathWorks, Inc., Natick, MA, USA), fitted by third degree polynomial fit (CurveFitting Toolbox, Matlab). A comparison of mutant versus control was done by using the unpaired two-tailed *t*-test ($^*P > 0.01$, $^{**}P > 0.001$, $^{***}P \leq 0.001$).

Optical Coherence Tomography (OCT)

In vivo OCT (Bioptigen, Research Triangle Park, NC, USA) was performed directly after ERG measurement under the same anesthesia and pupil dilation. Retinas were scanned subsequently by using additional methylcellulose for lubrication. The OCT lens was advanced toward the eye until the retina appeared on the monitor, focused, leveled, and oriented with the optic nerve centered. The OCT image was captured using a rectangular volume scan (20 B-scan 1 frame). Images were imported as stacks in ImageJ (National Institutes of Health, Bethesda, MD, USA). The StackReg plugin was used to remove image distortion due to respiration of the animal.[24] All slices were merged by using "Z project" and "Sum Slices". Retinal layers were measured manually 500 μm from the center of the optic nerve[25] (Supplementary Fig. S1A). Data processing was done in Matlab. Statistical comparisons of mutant mice versus WT littermates were done using a Holm-Šidák test[26,27] and a comparison of P25 versus other ages via a Dunnets multiple comparison[28] (Supplementary Fig. S1; Supplementary Table S1), with both following ANOVA ($^*P > 0.01$, $^{**}P > 0.001$, $^{***}P \leq 0.001$).

Optomotor Response (OMR)

The OMR was recorded using a quantitative OMR setup (Phenosys, Berlin, Germany), which allows for measurement and analysis of responses in freely moving mice. Visual stimuli were presented on a rotating virtual sphere surrounding the animal, consisting of gratings of 13 different spatial frequencies between 0.0125 and 0.5 cyc/deg. Meanwhile, the mouse was recorded and video tracked online to automatically maintain the distance of the animal to the virtual sphere and, therefore, the perceived spatial frequency.[29,30] Each stimulus was presented for 60 seconds. The automated tracking was used to quantitatively evaluate all experiments. Stimulus-correlated head movements were determined, and the ratio of movements within a velocity range of 2 to 14 deg/s in the correct direction divided by movements in the same range in the incorrect direction were calculated and defined as the OMR (OMRindex). Each set of stimuli was presented three times in a pseudo-randomized order with resting time of a minimum of 1 hour between trials. Data analysis was done using the quantitative OMR software and Matlab.

Table. qRT-PCR Primers

Gene	Species	Forward	Reverse
GAPDH	Human	GAGTCAAGGGATTTGGTCGT	TTGATTTTGGAGGGATCTCG
BBS5	Human	ACAACAAGGACTGCTAACTCTAAA	GTACTGCCATCACAGAAGTAAAAA
Gapdh	Mouse	CGACTTCAACAGCAACTCCCACTCTTCC	TGGGTGGTCCAGGGTTTCTTACTCCTT
Bbs1	Mouse	CCCTACTTCAAGTTCAGCCTG	TCTGCCTTTTCCCTGATGTC
Bbs2	Mouse	ACATTGCCCCACCTCTTG	TCTTCCCATCACCGTCAAAG
Bbs4	Mouse	GCTCCAGACTTCCCTATTGTG	GCATATTCACATAGCCCCTGAG
Bbs7	Mouse	ATGGATCTGACGTTAAGCCG	CCTTTTGTGTAGCCCTTTGTCTTGAGGT
Bbs9	Mouse	ACAAATCTCCTGTCAGTCTGC	TCGTTGGGATGTTCTGGAAG
Bbs18	Mouse	CCCTTAAAATCTCTGACGCTGG	TGCCTTTTCTGCCATTTCTTG

To determine the range of stimulus uncorrelated activity of all animals (baseline), we calculated the interquartile interval for the OMR for all mice at 0.5 cyc/deg, a spatial frequency not perceivable by the animals. (OMRindex, 1.15; yellow area in Figs. 2, 5, 8).[31] The spatial frequency threshold was then calculated as the intersection of polynomial fit (third degree) with this baseline interval.

Gene and Protein Expression Analysis

hTERT-RPE1 cells (ATCC) were cultured in Dulbecco's modified Eagle's medium (DMEM)-F12 (Thermo Fisher Scientific, Waltham, MA, USA) supplemented with heat-inactivated 10% fetal bovine serum (FBS, LONZA, Cologne, Germany), and 1% penicillin/streptomycin (P/S, Thermo Fisher Scientific). Knockdown (KD) was performed using BBS5 small interfering RNA (siRNA) (hs.Ri.BBS5.13; IDT, Leuven, Belgium) and BBS8 siRNA (HSc.RNAI.N198309.12; IDT). Nontargeting siRNA (DS-NC1; IDT) was used as control. siRNA transfections were performed in 6-well plates with the Lipofectamine RNAiMax transfection reagent (13778150; Thermo Fisher Scientific) according to the manufacturer's instructions.

To confirm KD, RNA was extracted from hTERT-RPE1 cells using TRIzol reagent (15596026; Thermo Fisher Scientific) following the manufacturer's instructions. RNA was transcribed into cDNA with the GoScript reverse transcription system (A5000; Promega, Mannheim, Germany). The StepOnePlus Real-Time PCR system (4376600; Thermo Fisher Scientific) was used to perform quantitative real-time PCR (qRT-PCR) using SYBR green (Platinum SYBR green qPCR SuperMix-UDG, 11733046; Thermo Fisher Scientific; for primers see Table) according to manufacturer's recommendation and as described previously.[32] Relative target gene expression was normalized to glyceraldehyde 3-phosphate dehydrogenase (GAPDH), and data were analyzed by the comparative cycle threshold or $2^{\Delta\Delta CT}$ method.

For gene expression analysis in mouse retina (6 months old), eyes were enucleated and immersed in cold phosphate-buffered saline (PBS). Retinas were removed followed by RNA isolation, cDNA synthesis, and qRT-PCR as described above.

For protein analysis using Western blotting, cells were lysed in RIPA buffer with EDTA-free protease inhibitor cocktail (Halt Protease and Phosphatase Inhibitor Cocktail [100×]; Thermo Fisher). Proteins were then denatured in Laemmli buffer, resolved using 10% SDS PAGE, and transferred to a polyvinylidene fluoride membrane (Immobilon-FL polyvinylidene fluoride membrane, 05317; Sigma, Darmstadt, Germany). Membranes were blocked with Applichem blocking buffer (0.2% AppliChem blocking reagent, 10 mM TrisHCl, 150 mM NaCl, and 0.04% NaN3 in ddH2O; pH 7.4) and probed with primary antibodies (β-catenin, D10A8; Cell Signaling Technology, Frankfurt, Germany and GAPDH, TA802519; Origene, Herford, Germany). Blots were scanned using the Odyssey infrared imaging system (LI-COR Biosciences, Lincoln, NE, USA).

Immunocytochemistry

For the immunofluorescence analysis, cells were fixed in 4% paraformaldehyde for 10 minutes, permeabilized for 15 minutes in PBS substituted with 0.3% Triton X-100 and blocked for 1 hour at room temperature with blocking buffer containing 0.1% ovalbumin and 0.5% fish gelatin. Cells were incubated overnight at 4°C with the primary antibody (anti-phospho-histone H2AX [Ser139] antibody, clone JBW301; Merck Millipore, Darmstadt, Germany), followed by washing in PBS for 30 minutes. Secondary antibodies (Alexa Fluor 555; Molecular Probes, Eugene, OR, USA), and DAPI were added and incubated for 1 hour at room temperature before mounting. A DM6000B microscope (Leica, Bensheim, Germany) was used to image the specimens. Images were deconvoluted with Leica imaging software (BlindDeblur Algorithm, one iteration step). Images processing and intensity measurements were performed using Fiji/ImageJ software (National Institutes of Health).

Results

Retinal Characterization of Aging *Bbs6*$^{-/-}$ Mice

OCT analysis of *Bbs6*$^{-/-}$ mice showed that the loss of retinal thickness was predominantly driven by the loss of photoreceptor cells. In littermate control mice (*Bbs6*$^{+/+}$), retinal layers were clearly distinguishable (Supplementary Fig. S1). Dense layers such as the RPE or ganglion cell layer appeared lighter and less dense areas such as the inner and outer nuclear layer (INL and ONL, respectively) appeared darker. The thickness of the retina in *Bbs6*$^{+/+}$ as well as all individual retinal layers remained constant over time until the latest age tested, P205 (Supplementary Fig. S1B; Supplementary Table S1).

Compared to the control, the retina thickness of *Bbs6*$^{-/-}$ mice was already decreased at P25 and continued to decrease over time (Fig. 1). To highlight the changes, the data were normalized to the control mice of the same age. A direct comparison is shown in Supplementary Figure S1. Significant differences in thickness only appeared in the outer layers, especially the ONL, as well as the inner segments (ISs) and OSs of the photoreceptors. Already at P25, the ONL thickness was reduced to 80% and continued to decrease to ∼35% at P205. The increase of the ONL at P175 is due to normalization against the control at this age (Supplementary Fig. S1B). The OS showed the biggest difference compared to *Bbs6*$^{+/+}$ at P25, with a thickness reduced to 60%, progressing to 20% at P175. In contrast, the ISs only began to shorten significantly at P115 (reduction to 40% of the *Bbs6*$^{+/+}$).

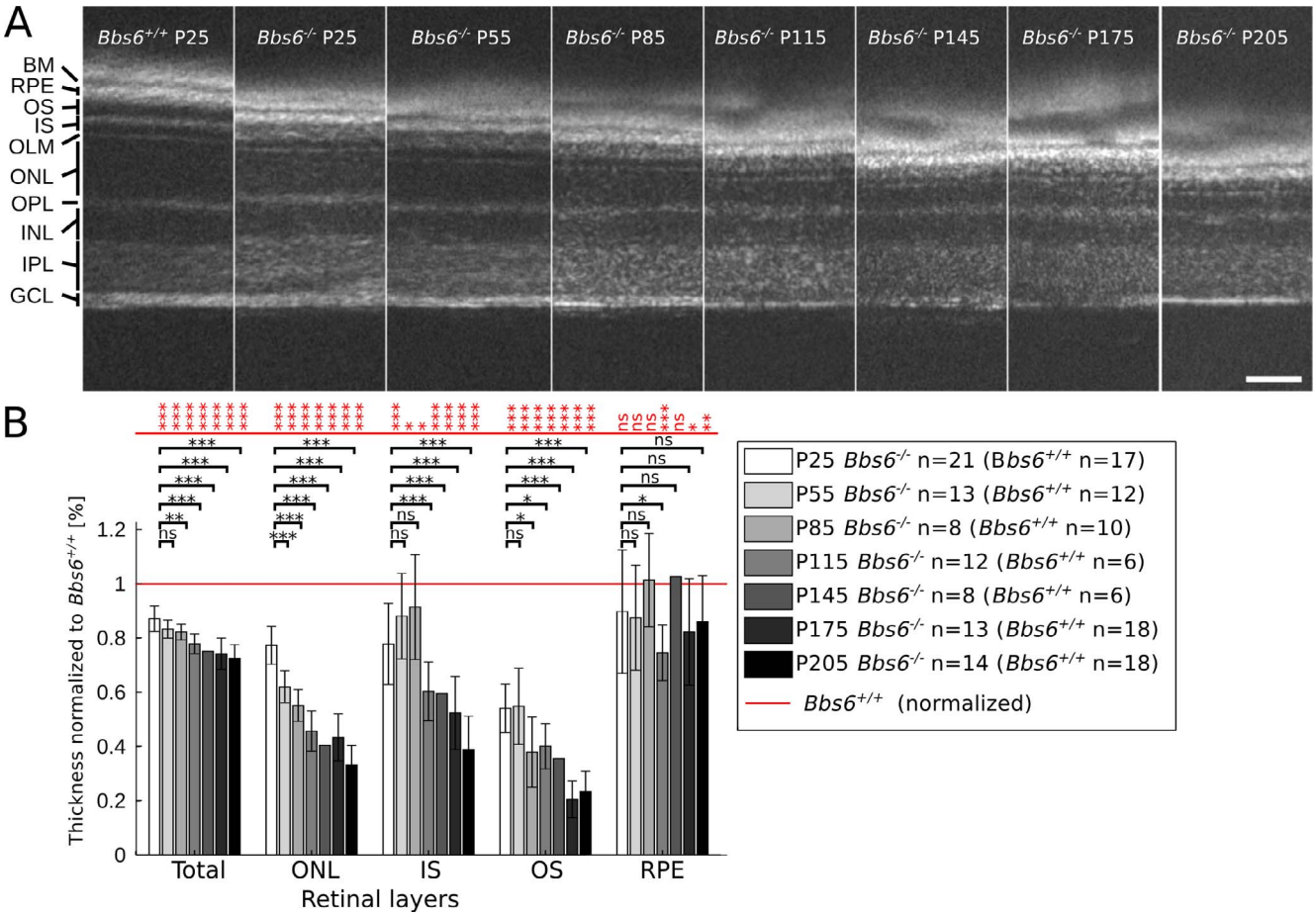

Figure 1. In vivo OCT scans of BBS6-deficient mice. Retinal thickness is measured at 500 μm distance to optic nerve. *Bbs6*$^{-/-}$ retina is already reduced at P25 and continues to decrease until P205 compared to control (**A**). Especially ONL, as well as IS and OS of the photoreceptors show a significant degression over time compared to *Bbs6*$^{+/+}$ (*red line*, **B**). Statistics were done using a Dunnets multiple comparison test, following ANOVA (*$P > 0.01$, **$P > 0.001$, ***$P \leq 0.001$). *Scale bar*: 50 μm.

There was no significant decrease in the thickness of the ganglion cell layer, the INL, the inner plexiform layer, or outer plexiform layers (Supplementary Fig. S1B). Looking specifically at the RPE, there was a significant difference between the control and *Bbs6*$^{-/-}$ at P115, P175, and P205 (red stars). However, the thickness of the RPE did not significantly change over time, as shown by a comparison of all ages to P25 (black stars).

A more global assessment of visual function is achieved via analysis of the OMR. The automatically determined spatial frequency response curves for *Bbs6*$^{+/+}$ and *Bbs6*$^{-/-}$ from ages P25 to P205 are displayed in Figure 2. *Bbs6*$^{+/+}$ mice exhibited behavior that lead to an OMR above 1.4 at 0.2 cyc/deg, which remained constant in the aging mice. The threshold remained around 0.4 cyc/deg. In contrast, the curve of *Bbs6*$^{-/-}$ mice declined over time. The spatial frequency threshold was already slightly reduced at P25 and declined significantly from 0.37 cyc/deg to 0.33 cyc/deg by P205.

ERG recordings of mice were measured after administering light flashes of six different intensities under both dark-adapted (scotopic) and photopic conditions (see Supplementary Fig. S2A). As expected, with increased light intensity, the response of the photoreceptors (a-wave) showed an increasingly negative current, whereas the secondary neurons (mainly on-bipolar cells, b-wave; Supplementary Fig. S2A) exhibited increasingly positive currents.[33] Representative ERG traces for *Bbs6*$^{+/+}$ and *Bbs6*$^{-/-}$ mice under photopic (30 cd/cm^2) and scotopic (1 cd/cm^2) conditions are shown in Figure 3A. A- and b-wave amplitudes measured at these conditions are plotted in Figures 3B through 3E. The *Bbs6*$^{+/+}$ mice showed an increased photopic (cone) response from age P25 to P85. Afterward, it remained mostly constant until day P175 (Figs. 3A, 3B). The b-wave was mostly constant until a slight degression, set in at P115 (Fig. 3A, left side, 3C). *Bbs6*$^{-/-}$ mice already showed lower cone responses as early as P25, which remained consistently low at around 8 μV across all ages tested. The b-wave amplitude in *Bbs6*$^{-/-}$ mice was already 20% lower than that in *Bbs6*$^{+/+}$ mice at P25, which declined to approximately 50% by P205.

An analysis of the scotopic responses of dark-adapted *Bbs6*$^{-/-}$ mice still showed a rod response at P25, albeit significantly lower than that in *Bbs6*$^{+/+}$ mice. This response steadily declined to 24 μV by P205 compared to 148 μV in the *Bbs6*$^{+/+}$ mice at this age. The b-wave response of *Bbs6*$^{-/-}$ mice showed a steep descent followed by stable amplitudes around 400 μV after P85 (~60% of P25). The *Bbs6*$^{+/+}$ response showed a similar progression, yet the degree of decline was not as severe (~90% of P25).

Retinal Characterization of Aging *Bbs8*$^{-/-}$ Mice

Comparable to *Bbs6* knockout mice (encoding a putative chaperonin protein), the retina of *Bbs8* knockout mice (encoding a BBSome complex protein) also exhibited a significant degeneration of the outer retinal layers, as determined by OCT analysis (Fig. 4). Identical to the *Bbs6*

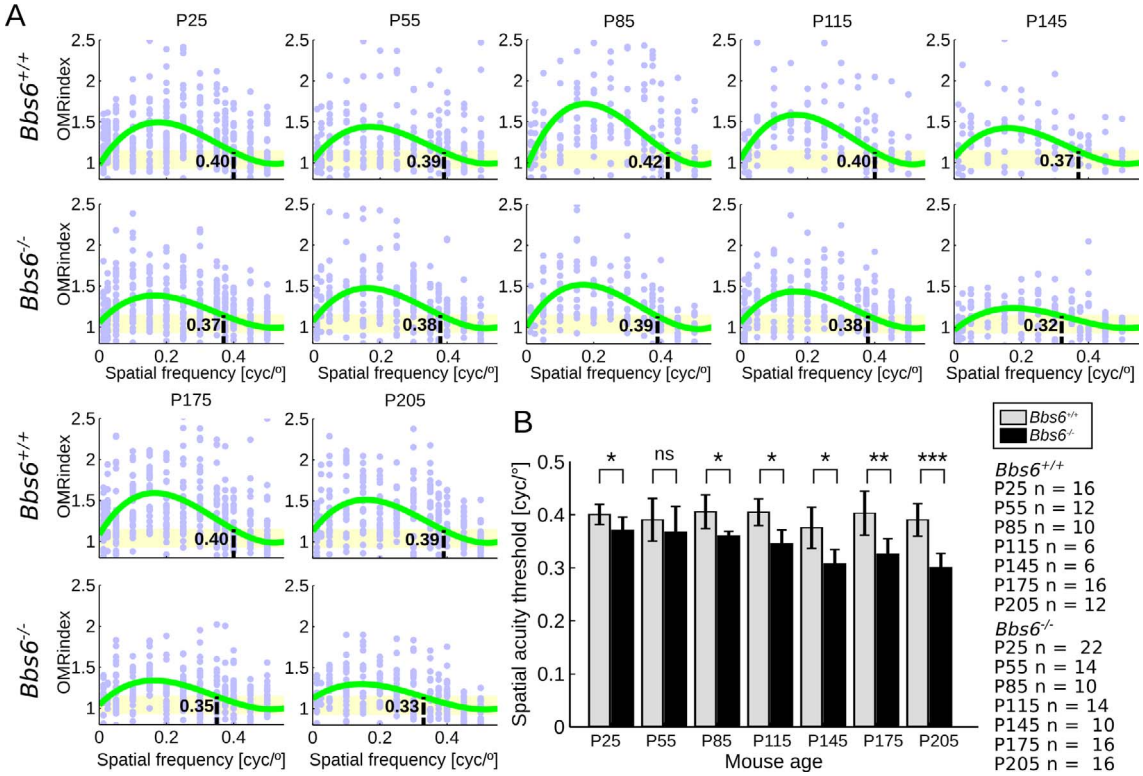

Figure 2. Visual acuity measured via OMR of *Bbs6* animals. Data points (purple) indicate OMR indeces for each mouse and each trial at 13 different spatial frequencies. The *yellow area* represents stimulus uncorrelated behavior calculated at 0.5 cyc/deg (OMRindex, 0.93–1.15 cyc/deg). *Dashed line* visualizes calculated spatial frequency threshold (OMRindex of polynomial fit below 1.15 cyc/deg). $Bbs6^{+/+}$ mice have a stable visual acuity curve with a maximum at 0.2 cyc/deg and a threshold around 0.4 cyc/deg (**A**). $Bbs6^{-/-}$ mice show a slightly lower curve already at P25, which declines significantly until P205, with thresholds declining to 0.33 cyc/deg. Comparison shows increasing differences between $Bbs6^{-/-}$ and control over time (**B**).

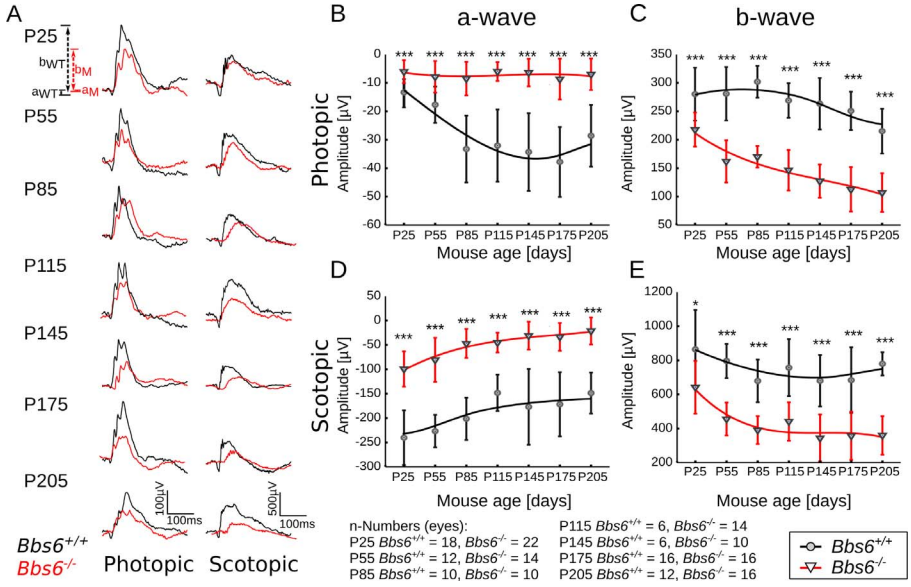

Figure 3. Representable traces of electric response of BBS6-deficient photoreceptors and downstream cells (*red trace*) compared to control (*black trace*) for photopic (**A**, *left panel*, at 30 cd s/m^2) and scotopic (**A**, *right panel*, 1 cd s/m^2) light stimulation show degression of responses from P25 to P205. The a-wave of $Bbs6^{-/-}$ cones remains small at a very low level (**B**). Downstream cells show a steep decline of responses from P25 to P205 compared to $Bbs6^{+/+}$. The scotopic ERG of $Bbs6^{-/-}$ is already reduced by 50% at P25 and falls to ~25% at P205 (**D**). The response of secondary neurons falls from ~75% to ~50% (**E**). Comparison of $Bbs6^{+/+}$ and $Bbs6^{-/-}$ was done by unpaired two-tailed *t*-test ($^*P > 0.01$, $^{**}P > 0.001$, $^{***}P \leq 0.001$).

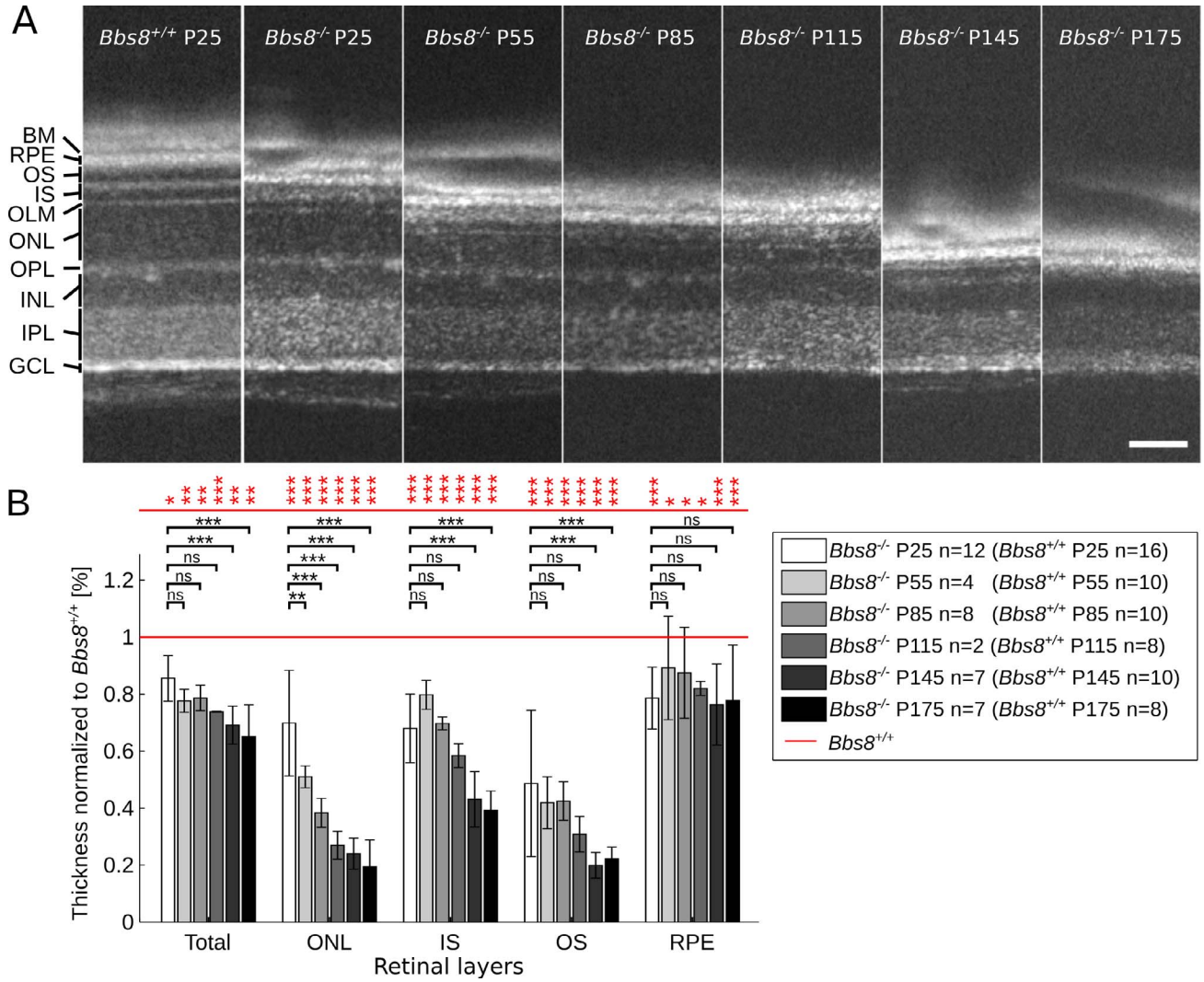

Figure 4. In vivo OCT scans of BBS8-deficient retina show a thinning of retina already at P25 which continues to manifest in smaller outer layers every 30 days (**A**). Especially the ONLs and OSs of the photoreceptors show a significant degression over time to about 20% compared to $Bbs8^{+/+}$ (*red line*) (**B**). ISs reduce to ~40% and RPE is reduced but show no significant further degression. Statistics were done using a Dunnets multiple comparison, following ANOVA ($^{*}P > 0.01$, $^{**}P > 0.001$, $^{***}P \leq 0.001$). *Scale bar*: 50 µm.

littermate controls ($Bbs6^{+/+}$), $Bbs8^{+/+}$ control retinas showed no significant decrease in thickness from P25 to P205 (Supplementary Fig. S1C; Supplementary Table S1). Yet in contrast to $Bbs6^{-/-}$, the decrease in photoreceptor layers in the $Bbs8^{-/-}$ mice was both faster and more extreme. Already by P25 the outer layers of $Bbs8^{-/-}$ mice were ~30% (ONL and IS) to 50% (OS) thinner than in littermate controls. This steadily continued, and by the latest age tested, the ONL and OS were reduced to 20% of $Bbs8^{+/+}$. Intriguingly, although the thickness of the RPE was unchanged in the *Bbs6* mutants, in $Bbs8^{-/-}$ it was reduced to 80% from the beginning (P25) and remained as such, showing no progression of degeneration.

The increased loss of retinal thickness also corresponded to a more rapid loss of visual function in *Bbs8* than the *Bbs6* mutants, as measured via the OMR. Consistent with the above findings, the WT control mice ($Bbs8^{+/+}$) exhibited a constant OMR above 1.4 at 0.2 cyc/dec and the threshold remained around 0.4 cyc/deg. The variation in amplitude of the OMRindex was due to the varying behavior of the freely moving mice (Fig. 5A). In $Bbs8^{-/-}$ mice, the spatial frequency threshold declined significantly, and at P175, the amplitude of the OMRindex barely rose above chance (upper interquartile interval of all mice at 0.5 cyc/deg; yellow area in Fig. 5A), resulting in a threshold of 0.28 cyc/deg. These data were consistent with the observed loss of retinal thickness.

To determine the physiologic responses of the different cell types, ERG recordings of *Bbs8* mutant mice were measured as for *Bbs6* mutant mice. Similarly, representative ERG traces for $Bbs8^{+/+}$ and $Bbs8^{-/-}$ mice under photopic (30 cd/cm^2) and scotopic (1 cd/cm^2) conditions are shown in Figure 6A. A- and b-wave amplitudes measured at these conditions are plotted in Figures 6B through 6E. The electrical response of the cones and secondary neurons after photopic stimulation remained stable over time in $Bbs8^{+/+}$ mice. In contrast, $Bbs8^{-/-}$ mice never exhibited a cone response. Thus follows, the b-wave was also nonexistent because without any input from cones there cannot be any electrical response from secondary neurons.

However, an albeit diminished scotopic response remained in the $Bbs8^{-/-}$ mice. This declined consistently by 80% between P25 and P175 to an almost undetectable response. The b-wave declined similarly by 62% between P25 and P175.

Comparing the progression of retinal degeneration in *Bbs6*- versus *Bbs8*-deficient mice revealed subtle differences in pathogenic mechanisms, reflecting their distinct molecular

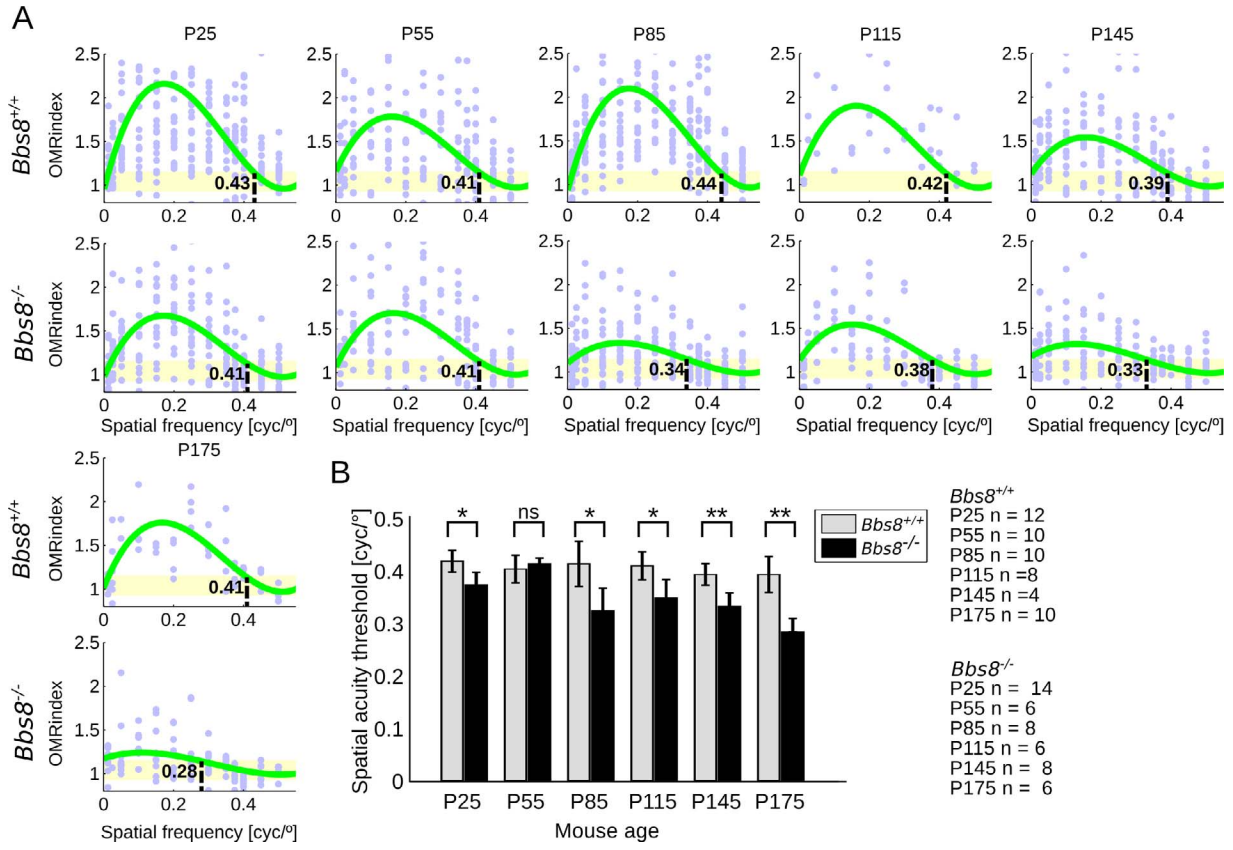

Figure 5. Optomotor response curves for *Bbs8* mice. Single measurement data points (*purple*) show a for unrestrained animals normal jitter. Maxima of visual acuity curve are around 0.2 cyc/deg. Calculated spatial frequency threshold (*dashed line*, intersection of polynomial fit with stimulus uncorrelated behavior [*yellow area*, OMRindex, 0.93–1.15 cyc/deg]) show a stable value of around 0.4 cyc/deg from P25 to P175 in control mice compared to a declining threshold in $Bbs8^{-/-}$ down to 0.28 cyc/deg. Comparison shows increasing differences between $Bbs8^{-/-}$ and control over time (**B**).

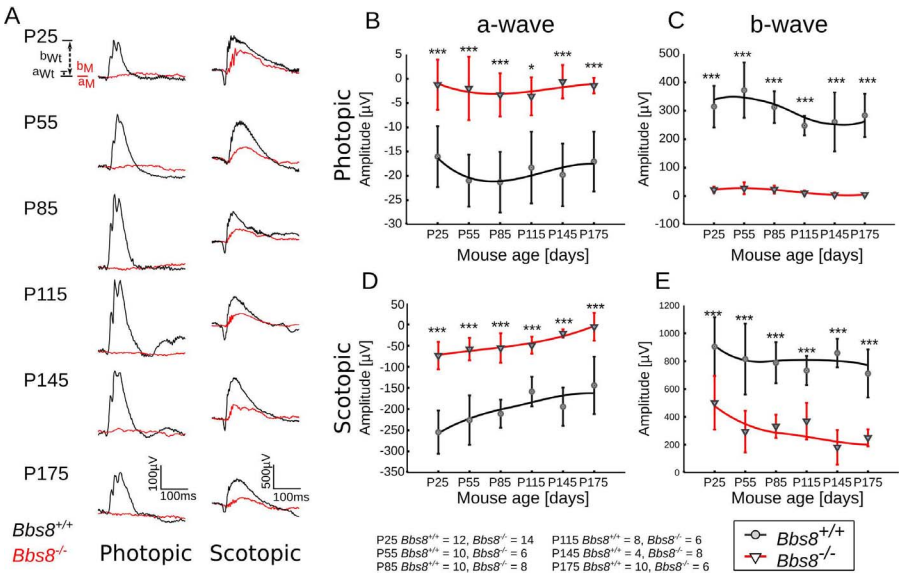

Figure 6. Representable traces for photopic ERGs show no a- or b-wave for $Bbs8^{-/-}$ mice (**A**, *left panel*, **B**, **C**, 30 cd s/m^2). Rods show reduced responses at P25 which decline over time (**A**, *right panel*, **D**, **E**, 1 cd s/m^2). Comparison of $Bbs8^{+/+}$ and $Bbs8^{-/-}$ was done by unpaired two-tailed *t*-test ($^*P > 0.01$, $^{**}P > 0.001$, $^{***}P \leq 0.001$).

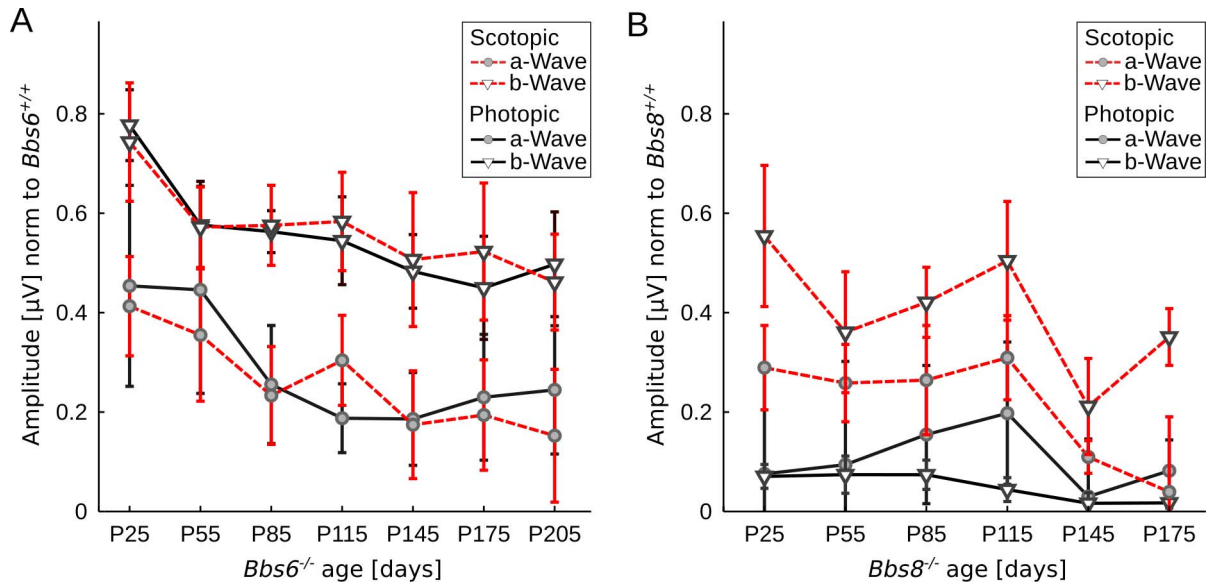

Figure 7. ERG responses normalized to *Bbs6*$^{+/+}$ show similar progression for rods (scotopic responses) and cones (photopic) from ~40% to ~25%, as well as the similar progression of their downstream cells (b-wave) from ~80% to ~50% of the *Bbs6*$^{+/+}$ at P205 (**A**). This is different in *Bbs8*$^{-/-}$ (**B**) where no photopic response was detectable. Photopic response decreases from 30% to 5% in cones and 60% to 40% in bipolar cells.

functions. In the *Bbs6*$^{-/-}$ mice, both photopic and scotopic ERG responses declined at a similar rate and some residual function remained in aged mice (P205; Fig. 7).

In contrast, the *Bbs8*$^{-/-}$ mice never displayed any photopic response, suggesting that cones failed to mature functionally. Even the scotopic response was greatly diminished and progressed more rapidly. Although the RPE was unchanged in the *Bbs6*$^{-/-}$ mice compared to control across all time points, the RPE in the *Bbs8*$^{-/-}$ mice was reduced from the beginning.

Retinal Characterization of Aging *Bbs5*$^{-/-}$ Mice

Because we saw striking differences between mouse knockouts of a BBS chaperone gene versus a BBSome gene, we wanted to see if this effect could be recapitulated when another component of the BBSome was knocked out. OCT analysis of *Bbs5*$^{-/-}$ retina revealed that most outer retinal layers were only minimally reduced (albeit significantly) compared to the control up to 5 months. Even by 10 months, there was no significant decline in the mutant compared to 2 months (Figs. 8A, 8B). Interestingly the thickness of the IS possibly showed an opposite effect, suggesting an elongation of the IS as the mice aged (10 months, note this time point is significant albeit with a large standard deviation). The extension of the IS might not be a direct cause of lengthening but rather a side effect of infiltration or replacement by inflammatory or gliotic material.

Visual function of the *Bbs5*$^{-/-}$ mutant as measured via OMR showed no significant reduction at 2 or 5 months of age compared to control and only a minimal deterioration as late as 10 months of age.

This result could be explained by the fact that although already decreased, there still remained 50% of the secondary neuron photopic response (photopic b-wave) at 5 months of age, as measured via ERG. Closer analysis of ERG response in the *Bbs5*$^{-/-}$ mutant revealed no significant change in scotopic response until 10 months of age. That suggests an initial development and maturation of functional cones unlike in the other BBSome mutant *Bbs8*.

Loss of BBS8 Leads to Reduced Expression of BBSome Transcripts. Because BBS8 and BBS5 are both components of the BBSome complex, required for intraflagellar trafficking, the striking difference in visual phenotype between the two mouse knockout models was unexpected. In our previous studies, we have shown that the loss of BBS8 results in altered gene expression of cilia-related proteins.[32] Therefore, we examined the impact of the loss of either *Bbs8* or *Bbs5* on the expression of other BBSome components in the retina via qRT-PCR. In contrast to a previous study that looked at BBS gene expression in developing retina and saw no differences,[34] we observed a significant reduction of *Bbs1*, *Bbs2*, *Bbs4*, *Bbs7*, and *Bbs9* mRNA levels in *Bbs8*$^{-/-}$ retina at 6 months of age compared to that of WT littermates (Fig. 9A). In contrast, the transcriptional levels of BBSome components remained stable in *Bbs5*$^{-/-}$ retina. The expression of *Bbs18* was not altered in either model. Because the loss of *Bbs8* lead to significant changes in gene expression of other BBSome components, it is likely more detrimental to cell physiology than the loss of *Bbs5*.

Lack of *BBS8* Causes Pronounced Defects in Cellular Physiology. To further elucidate the mechanistic differences between the role of BBS8 and BBS5, we turned to an in vitro culture system. We knocked down BBS8 and BBS5 in hTERT-RPE1 cells by using specific siRNAs. The level of KD was validated by qRT-PCR (Supplementary Fig. S3). Numerous studies including our own[32] have shown that the loss of BBS proteins affects proteasomal degradation of downstream targets, in particular β-catenin.[16,32,35] Western blot analysis of β-catenin levels in BBS8 and BBS5 KD cells confirmed that although levels of β-catenin were elevated in BBS5 KD cells compared to control, these were lower than in BBS8 KD (Fig. 9B).

Recent studies have implicated the role of DNA damage stress in the pathophysiology of ciliopathies.[36,37] High levels of endogenous phosphorylated histone γH2AX are indicative of cellular stress via genomic instability and/or defective DNA damage repair pathway. Our immunocytochemistry results showed that BBS8 KD cells exhibited higher expression levels of γH2AX than that of control cells (Figs. 9C, 9D). However, although the loss of BBS5 also increased levels of γH2AX expression, this was significantly lower than BBS8 KD cells. Combined, these findings support the hypothesis that the loss of BBS8 is likely more detrimental to the cell physiology than the loss of BBS5, which could lead to a higher cell death rate,

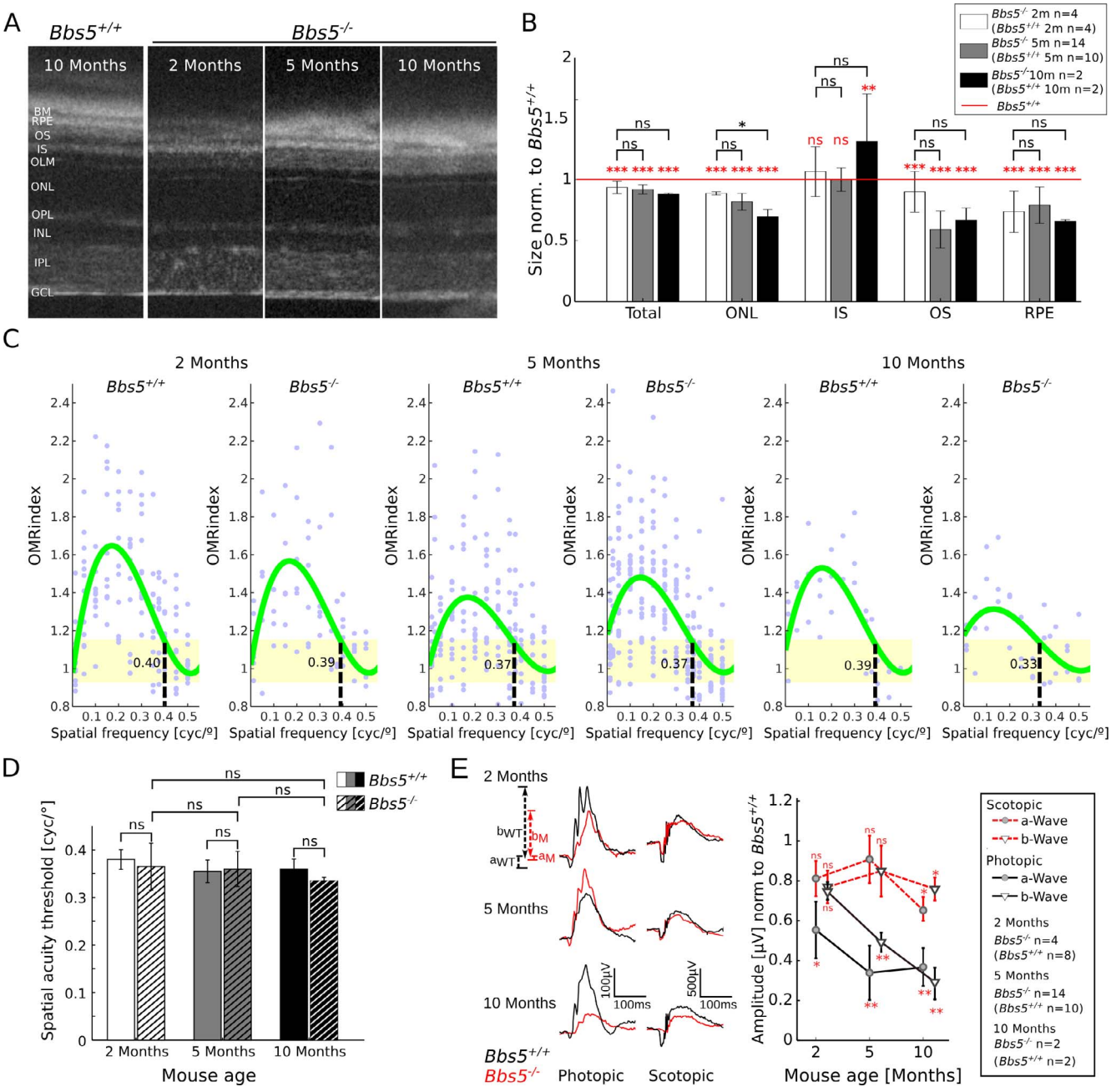

Figure 8. OCT images of *Bbs5*$^{-/-}$ show reduced thickness of retinal layers (**A**). Especially the outer layers are significantly thinner than *Bbs5*$^{+/+}$ (**B**, Holm-Sidak Test [*red stars*]), but no progression of retinal degeneration from 2 months to 10 months (unpaired two-tailed *t*-tests, *black stars*). Spatial frequency curves show slight differences in spatial frequency thresholds (**C**, intersection of polynomial fit and not stimulus correlated behavior [*yellow area*]) in *Bbs5*$^{-/-}$ compared to *Bbs5*$^{+/+}$, which does not decline significantly from 2 to 10 months (**D**). The ERGs of *Bbs5*$^{-/-}$ compared to *Bbs5*$^{+/+}$ show a significant reduction of cone responses (photopic a-wave) in 2-, 5-, and 10-month-old mice (**E**, *red stars*, unpaired two-tailed *t*-test). At 5 months also the downstream neurons (b-wave) show a significantly lower amplitude which decreases until 10 months. The scotopic responses of rods and bipolar cells show no significantly lower responses at 2 and 5 months but a slight reduction at 10 months (*$P > 0.01$, **$P > 0.001$, ***$P \leq 0.001$). *Scale bar*: 50 µm.

explaining why the loss of BBS8 has a more pronounced retinal phenotype.

Discussion

Retinal degeneration is not only the most common phenotype among ciliopathy patients, but a large proportion of non-syndromic retinal disorders are linked to defects in cilia genes.[38,39] So far no treatment strategies to target cilia-related defects in the visual system are clinically available. Because many ciliopathy mouse models generated to date recapitulated the retinal degeneration observed in patients, these models have proven to be powerful tools to study the effect of specific gene inactivation on retinal function.[40–44]

BBS is considered an archetypical ciliopathy, and defects in BBS-causing genes results in defective ciliary trafficking and consequent function. Thus, any insights gained from studying BBS mouse models are likely applicable to other syndromic and

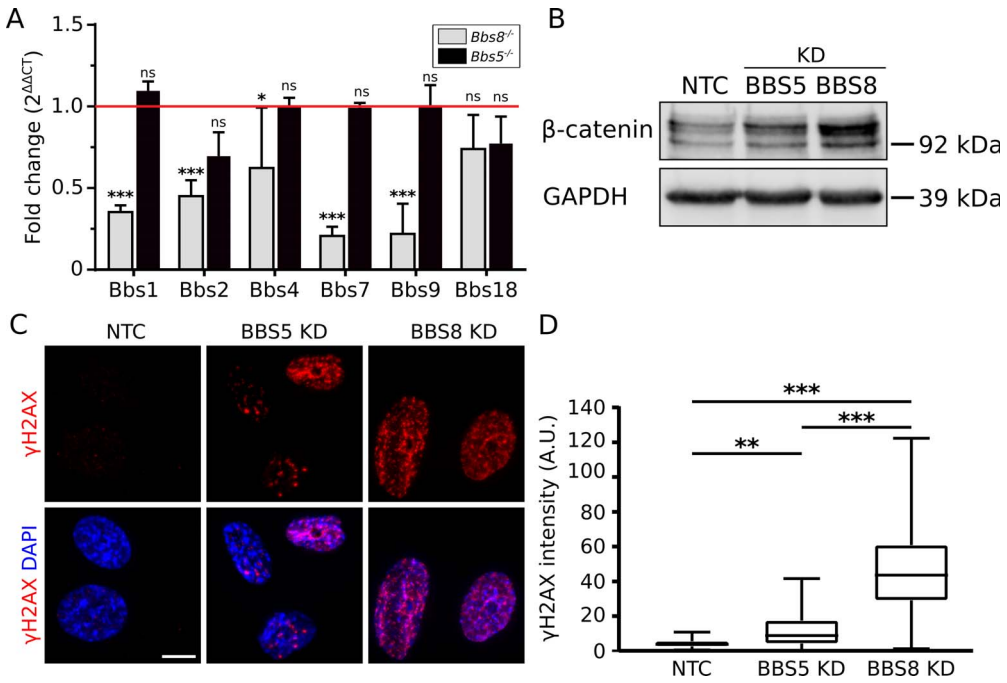

FIGURE 9. Lack of BBS8 causes pronounced defects in cellular physiology. *Bbs8*$^{-/-}$ mouse retina show significantly lower mRNA levels of *Bbs1*, *Bbs2*, *Bbs4*, *Bbs7*, and *Bbs9* than WT (**A**, *red line*). The transcriptional levels of these BBSome components remained stable in *Bbs5*$^{-/-}$ retina. Expression of *Bbs18* was not altered in either model. β-Catenin levels are slightly elevated upon BBS5 KD and much higher in BBS8 KD hTERT-RPE1 cells compared to control cells (NTC, nontargeting siRNA) (**B**). BBS5 and BBS8 KD cells exhibited higher levels of γH2AX than that of control cells (**C**), which was significantly higher in BBS8 KD than BBS5 KD cells (**D**) ($^{*}P > 0.01$, $^{**}P > 0.001$, $^{***}P \leq 0.001$). *Scale bar*: 10 μm.

nonsyndromic retinal degenerations. We closely characterized the rate of visual decline in a selection of different BBS mouse models. Although numerous reports have previously described various aspects of visual function in a variety of BBS mouse models, none have systematically compared different methods of visual assessments followed closely over time.[17,22,40,45–51] Such systematic characterization over time is essential as a benchmark for finding the right time point at which to test different treatment options.

Similar to previously published *Bbs* mutant mouse models, we saw that the complete loss of BBS5, BBS6, or BBS8 leads to different rates of retinal degeneration over time with somewhat varying phenotypic differences. This difference in the development and rate of degeneration could be explained by their different molecular functions. BBS6/MKKS is a putative chaperonin complex protein, responsible for the correct folding and function of other ciliary proteins, whereas BBS5 and BBS8 are BBSome complex proteins required for ciliary trafficking.[23,52,53] Thus, it is particularly intriguing that the phenotype of these two knockout mice (*Bbs5*$^{-/-}$ and *Bbs8*$^{-/-}$) are so dramatically different, suggesting either alternative nonoverlapping functions or varying rates of redundancy and compensation among the BBSome complex proteins. BBS8-deficient retina degenerate rapidly and the mice are mostly blind after less than 6 months of age. In contrast, *Bbs5*$^{-/-}$ mice exhibit a mild rate of retinal degeneration and vision is "relatively" unaffected even by 10 months. Not only in the retina does the phenotype differ so dramatically; although BBS8-deficient mice show a small tendency to become obese[22], *Bbs5*$^{-/-}$ mice rapidly become extremely overweight (Hernandez-Hernandez, unpublished data, 2018). Therefore, each of these BBSome proteins must have different purposes dependent on tissue expression.

In support of alternative nonoverlapping functions and/or varying rates of redundancy and compensation among the BBSome complex proteins, we found that the loss of BBS8 was more detrimental to cell physiology than the loss of BBS5, both in vivo and in vitro. In mouse retinas, the loss of BBS8 lead to significant changes in gene expression of other BBSome components, which were unchanged upon the loss of BBS5. In cell culture, KD of BBS8 lead to an increased proteasomal dysfunction and cellular stress response compared to KD of BBS5. These differences in cellular responses could explain why the loss of BBS8 is more damaging to cell homeostasis and, therefore, has a more pronounced effect on photoreceptor survival. Our findings are in contrast to the study by Dilan et al.[34] that showed no differences in BBS gene expression in the developing retina. This suggests that the loss of *Bbs8* does not affect gene expression levels of other BBS genes per se but rather that the loss of *Bbs8* affects BBSome protein stability and, in consequence, mRNA expression over time. Because gene expression levels are not altered in *Bbs5* knockout mice, it would suggest that BBSome stability is less affected.

Close consideration of the difference between the phenotypes of the three different mouse models reveals subtle but important differences relating to their function and their hierarchy in the BBSome complex. An example of this is the complete loss of cone function in *Bbs8*$^{-/-}$ mice. Even at the earliest time point measured (P25), we found no photopic response upon ERG stimulation. This is in accordance with the retina-specific *Bbs8*$^{-/-}$ model analyzed by Dilan et al.,[34] who also found no photopic response at an earlier time point (P16). This suggests that Bbs8 is required for cone photoreceptors to reach functional maturity, although they are still able to develop (May-Simera, unpublished data, 2017).[34] Intriguingly, when *Bbs8* is only knocked out in cone photoreceptors, they are able to illicit a response at P30, suggesting that functional maturity of the cones is likely assisted by surrounding cell types.[34]

In the *Bbs8* congenital knockout mouse model from Hsu et al.,[50] the authors only measured the scotopic ERG responses, wherefore no statement could be made about their photopic response. Similar to our data, they observed that the a-wave and

b-wave steadily declined from 1 month onward. Yet, they still saw an increase in response at earlier time points (between P15 and 1 month), suggesting that the rod photoreceptors still attempt to develop but that the retinal rod response never reached the functionality of their littermate controls. Despite these being different mouse models, generated using different knockout strategies and on different background strains, we still see a similar decline of the scotopic response, validating both data sets.

The contribution of other ocular cell types to the visual phenotype can also be extrapolated to the RPE. We have previously seen that the primary cilium is important for RPE maturation.[16] In our data, we saw that already at a very young age the thickness of the RPE is consistently decreased in *Bbs8* and *Bbs5* (but not *Bbs6*) mutant mice in comparison to control, which could imply a defective RPE is contributing to a more pronounced visual phenotype. Identifying such unique differences could assist in the development and optimization of personalized treatment strategies for specific gene mutations.

Finally, our data highlight the importance of using a combinatorial approach for an assessment of visual function, in the context of categorizing the effect of gene mutations and potential therapeutic approaches. In the *Bbs5*$^{-/-}$ retina, there is only a minimal histologic change between 2 and 10 months of age, as observed by OCT. However, we are able to detect significant changes when it comes to ERG function. Conversely, in early *Bbs6*$^{-/-}$ retina there is a highly significant loss of outer retina thickness, yet ERG and OMR function seem virtually unaffected.

Retinal degenerative diseases can potentially be treated by gene replacement therapies,[17,18,44,51,54–56] yet this approach is also fraught with difficulties, and there is a study proposing that overexpression of BBS1 in the retina could be challenging.[18] The application of substances or alternative cell-based therapies, such as read through of nonsense mutation via translation inducing read through drugs[57] and induced pluripotent stem cell-derived cell replacement,[58–60] could offer alternative solutions. It has already been shown that restoration of BBSome function can correct an OS malformation if applied prior to full retinal maturation.[44] This occurs in mouse between P9 and P25, whereas in humans is only reached between the age of two to five years.[45,55] For each of the different treatment strategies, the time frame of application and measure of therapeutic outcome must be closely considered. For this, the mouse models analyzed in this study show distinct and diverging courses of degeneration, which can be used as a benchmark to test therapeutic interventions aimed at targeting retinal degeneration caused by cilia dysfunction.

Acknowledgments

The authors thank Petra Gottlöber for her technical assistance and Lena Brücker and Ann-Kathrin Volz for critical reading of the manuscript. They would also like to acknowledge the unwavering commitment of the animal care teams at the Johannes Gutenberg University of Mainz that made this research possible.

Supported by Alexander von Humboldt Foundation, Johannes Gutenberg University, Mainz, Germany, and Deutsche Forschungsgemeinschaft Grant MA 6139/3-1.

Disclosure: **V. Kretschmer**, None; **S.R. Patnaik**, None; **F. Kretschmer**, None; **M.M. Chawda**, None; **V. Hernandez-Hernandez**, None; **H.L. May-Simera**, None

References

1. Forsythe E, Beales PL. Bardet-Biedl syndrome. *Eur J Hum Genet*. 2013;21:8–13.
2. Weihbrecht K, Goar WA, Pak T, et al. Keeping an eye on Bardet-Biedl syndrome: a comprehensive review of the role of Bardet-Biedl syndrome genes in the eye. *Med Res Arch*. 2017; 5:10.18103/mra.v5i9.1526.
3. Ansley SJ, Badano JL, Blacque OE, et al. Basal body dysfunction is a likely cause of pleiotropic Bardet–Biedl syndrome. *Nature*. 2003;425:628–633.
4. Li JB, Gerdes JM, Haycraft CJ, et al. Comparative genomics identifies a flagellar and basal body proteome that includes the BBS5 human disease gene. *Cell*. 2004;117:541–552.
5. Jin H, White SR, Shida T, et al. The conserved bardet-biedl syndrome proteins assemble a coat that traffics membrane proteins to Cilia. *Cell*. 2010;141:1208–1219.
6. Zhang Q, Yu D, Seo S, Stone EM, Sheffield VC. Intrinsic protein-protein interaction-mediated and chaperonin-assisted sequential assembly of stable bardet-biedl syndrome protein complex, the BBSome. *J Biol Chem*. 2012;287:20625–20635.
7. Loktev AV, Zhang Q, Beck JS, et al. A bbsome subunit links ciliogenesis, microtubule stability, and acetylation. *Dev Cell*. 2008;15:854–865.
8. Slavotinek AM, Stone EM, Mykytyn K, et al. Mutations in MKKS cause Bardet-Biedl syndrome. *Nat Genet*. 2000;26:15–16.
9. Stoetzel C, Muller J, Laurier V, et al. Identification of a novel BBS gene (BBS12) highlights the major role of a vertebrate-specific branch of chaperonin-related proteins in Bardet-Biedl syndrome. *Am J Hum Genet*. 2007;80:1–11.
10. Seo S, Baye LM, Schulz NP, et al. BBS6, BBS10, and BBS12 form a complex with CCT/TRiC family chaperonins and mediate BBSome assembly. *Proc Natl Acad Sci U S A*. 2010;107:1488–1493.
11. Álvarez-Satta M, Castro-Sánchez S, Valverde D. Bardet-Biedl syndrome as a chaperonopathy: dissecting the major role of chaperonin-like BBS proteins (BBS6-BBS10-BBS12). *Front Mol Biosci*. 2017;4:55.
12. Slavotinek AM. *McKusick-Kaufman Syndrome. GeneReviews®*. Seattle: University of Washington; 1993.
13. Hulleman JD, Nguyen A, Ramprasad VL, et al. A novel H395R mutation in MKKS/BBS6 causes retinitis pigmentosa and polydactyly without other findings of Bardet-Biedl or McKusick-Kaufman syndrome. *Mol Vis*. 2016;22:73–81.
14. May-Simera H, Nagel-Wolfrum K, Wolfrum U. Cilia - the sensory antennae in the eye. *Prog Retin Eye Res*. 2017;60: 144–180.
15. Bonilha VL, Rayborn ME, Bhattacharya SK, et al. The retinal pigment epithelium apical microvilli and retinal function. *Adv Exp Med Biol*. 2006;572:519–524.
16. May-Simera HL, Wan Q, Jha BS, et al. Primary cilium-mediated retinal pigment epithelium maturation is disrupted in ciliopathy patient cells. *Cell Rep*. 2018;22:189–205.
17. Mockel A, Obringer C, Hakvoort TBM, et al. Pharmacological modulation of the retinal unfolded protein response in Bardet-Biedl syndrome reduces apoptosis and preserves light detection ability. *J Biol Chem*. 2012;287:37483–37494.
18. Seo S, Mullins RF, Dumitrescu AV, et al. Subretinal gene therapy of mice with Bardet-Biedl syndrome type 1. *Invest Ophthalmol Vis Sci*. 2013;54:6118–6132.
19. May-Simera HL, Gumerson JD, Gao C, et al. Loss of MACF1 abolishes ciliogenesis and disrupts apicobasal polarity establishment in the retina. *Cell Rep*. 2016;17:1399–1413.
20. Smith TS, Spitzbarth B, Li J, et al. Light-dependent phosphorylation of Bardet-Biedl syndrome 5 in photoreceptor cells modulates its interaction with arrestin1. *Cell Mol Life Sci*. 2013;70:4603–4616.
21. Dickinson ME, Flenniken AM, Ji X, et al. High-throughput discovery of novel developmental phenotypes. *Nature*. 2016; 537:508–514.
22. Ross AJ, May-Simera HL, Eichers ER, et al. Disruption of Bardet-Biedl syndrome ciliary proteins perturbs planar cell polarity in vertebrates. *Nat Genet*. 2005;37:1135–1140.

23. Tadenev ALD, Kulaga HM, May-Simera HL, Kelley MW, Katsanis N, Reed RR. Loss of Bardet-Biedl syndrome protein-8 (BBS8) perturbs olfactory function, protein localization, and axon targeting. *Proc Natl Acad Sci U S A*. 2011;108:10320–10325.
24. Thevenaz P, Ruttimann UE, Unser M. A pyramid approach to subpixel registration based on intensity. *IEEE Trans Image Process*. 1998;7:27–41.
25. Berger A, Cavallero S, Dominguez E, et al. Spectral-domain optical coherence tomography of the rodent eye: highlighting layers of the outer retina using signal averaging and comparison with histology. Stitt A, ed. *PLoS One*. 2014;9:e96494.
26. Holm S. A simple sequentially rejective multiple test procedure. *Scand J Stat*. 1979;6:65–70.
27. Seidler J. The life and work of Zbynek Sidak. *Appl Math*. 2000; 45:321–336.
28. Dunlap WP, Marx MS, Agamy GJ. FORTRAN IV functions for calculating probabilities associated with Dunnett's test. *Behav Res Methods Instrum*. 1981;13:363–366.
29. Kretschmer F, Sajgo S, Kretschmer V, Badea TC. A system to measure the optokinetic and optomotor response in mice. *J Neurosci Methods*. 2015;256:91–105.
30. Kretschmer F, Kretschmer V, Kunze VP, Kretzberg J. OMR-Arena: automated measurement and stimulation system to determine mouse visual thresholds based on optomotor responses. *PLoS One*. 2013;8:e78058.
31. Kretschmer F, Tariq M, Chatila W, Wu B, Badea TC. Comparison of optomotor and optokinetic reflexes in mice. *J Neurophysiol*. 2017;118:300–316.
32. Patnaik SR, Kretschmer V, Brücker L, et al. Bardet–Biedl syndrome proteins regulate cilia disassembly during tissue maturation. *Cell Mol Life Sci*. 2019;76:757–775.
33. Robson JG, Frishman LJ. Dissecting the dark-adapted electroretinogram. *Doc Ophthalmol*. 1998;95:187–215.
34. Dilan TL, Singh RK, Saravanan T, et al. Bardet-Biedl syndrome-8 (BBS8) protein is crucial for the development of outer segments in photoreceptor neurons. *Hum Mol Genet*. 2018; 27:283–294.
35. Gerdes JM, Liu Y, Zaghloul NA, et al. Disruption of the basal body compromises proteasomal function and perturbs intracellular Wnt response. *Nat Genet*. 2007;39:1350–1360.
36. Johnson CA, Collis SJ. Ciliogenesis and the DNA damage response: a stressful relationship. *Cilia*. 2016;5:19.
37. Slaats GG, Saldivar JC, Bacal J, et al. DNA replication stress underlies renal phenotypes in CEP290-Associated Joubert syndrome. *J Clin Invest*. 2015;125:3657–3666.
38. Kenny J, Forsythe E, Beales P, Bacchelli C. Toward personalized medicine in Bardet–Biedl syndrome. *Per Med*. 2017;14: 447–456.
39. RetNet (2018). Available at: https://sph.uth.edu/retnet/.
40. Nishimura DY, Fath M, Mullins RF, et al. Bbs2-null mice have neurosensory deficits, a defect in social dominance, and retinopathy associated with mislocalization of rhodopsin. *Proc Natl Acad Sci U S A*. 2004;101:16588–16593.
41. Eichers ER, Abd-El-Barr MM, Paylor R, et al. Phenotypic characterization of Bbs4 null mice reveals age-dependent penetrance and variable expressivity. *Hum Genet*. 2006;120: 211–226.
42. Fath MA, Mullins RF, Searby C, et al. Mkks-null mice have a phenotype resembling Bardet–Biedl syndrome. *Hum Mol Genet*. 2005;14:1109–1118.
43. Estrada-Cuzcano A, Roepman R, Cremers FPM, den Hollander AI, Mans DA. Non-syndromic retinal ciliopathies: translating gene discovery into therapy. *Hum Mol Genet*. 2012;21:R111–R124.
44. Veleri S, Lazar CH, Chang B, Sieving PA, Banin E, Swaroop A. Biology and therapy of inherited retinal degenerative disease: insights from mouse models. *Dis Model Mech*. 2015;8:109–129.
45. Davis RE, Swiderski RE, Rahmouni K, et al. A knockin mouse model of the Bardet-Biedl syndrome 1 M390R mutation has cilia defects, ventriculomegaly, retinopathy, and obesity. *Proc Natl Acad Sci U S A*. 2007;104:19422–19427.
46. Zhang Q, Nishimura D, Seo S, et al. Bardet-Biedl syndrome 3 (Bbs3) knockout mouse model reveals common BBS-associated phenotypes and Bbs3 unique phenotypes. *Proc Natl Acad Sci*. 2011;108:20678–20683.
47. Mykytyn K, Mullins RF, Andrews M, et al. Bardet-Biedl syndrome type 4 (BBS4)-null mice implicate Bbs4 in flagella formation but not global cilia assembly. *Proc Natl Acad Sci U S A*. 2004;101:8664–8669.
48. Seo S, Zhang Q, Bugge K, et al. A novel protein LZTFL1 regulates ciliary trafficking of the BBSome and smoothened. *PLoS Genet*. 2011;7:e1002358.
49. Zhang Q, Nishimura D, Vogel T, et al. BBS7 is required for BBSome formation and its absence in mice results in Bardet-Biedl syndrome phenotypes and selective abnormalities in membrane protein trafficking. *J Cell Sci*. 2013;126:2372–2380.
50. Hsu Y, Garrison JE, Kim G, et al. BBSome function is required for both the morphogenesis and maintenance of the photoreceptor outer segment. *PLoS Genet*. 2017;13: e1007057.
51. Cognard N, Scerbo MJ, Obringer C, et al. Comparing the Bbs10 complete knockout phenotype with a specific renal epithelial knockout one highlights the link between renal defects and systemic inactivation in mice. *Cilia*. 2015;4:10.
52. Zhang Q, Yu D, Seo S, Stone EM, Sheffield VC. Intrinsic protein-protein interaction-mediated and chaperonin-assisted sequential assembly of stable Bardet-Biedl syndrome protein complex, the BBSome. *J Biol Chem*. 2012;287:20625–20635.
53. Nachury MV, Loktev AV, Zhang Q, et al. A core complex of BBS proteins cooperates with the GTPase Rab8 to promote ciliary membrane biogenesis. *Cell*. 2007;129:1201–1213.
54. Acland GM, Aguirre GD, Ray J, et al. Gene therapy restores vision in a canine model of childhood blindness. *Nat Genet*. 2001;28:92–95.
55. Maguire AM, Simonelli F, Pierce EA, et al. Safety and efficacy of gene transfer for leber's congenital amaurosis. *N Engl J Med*. 2008;358:2240–2248.
56. Simons DL, Boye SL, Hauswirth WW, Wu SM. Gene therapy prevents photoreceptor death and preserves retinal function in a Bardet-Biedl syndrome mouse model. *Proc Natl Acad Sci U S A*. 2011;108:6276–6281.
57. Nagel-Wolfrum K, Möller F, Penner I, Baasov T, Wolfrum U. Targeting nonsense mutations in diseases with translational read-through-inducing drugs (TRIDs). *BioDrugs*. 2016;30:49–74.
58. Miyagishima KJ, Wan Q, Corneo B, et al. In pursuit of authenticity: induced pluripotent stem cell-derived retinal pigment epithelium for clinical applications. *Stem Cells Transl Med*. 2016;5:1562–1574.
59. Lund RD, Wang S, Klimanskaya I, et al. Human embryonic stem cell–derived cells rescue visual function in dystrophic rcs rats. *Cloning Stem Cells*. 2006;8:189–199.
60. Lu B, Malcuit C, Wang S, et al. Long-term safety and function of rpe from human embryonic stem cells in preclinical models of macular degeneration. *Stem Cells*. 2009;27:2126–2135.

Investigative Ophthalmology & Visual Science